

Efficient scheduling of astronomical observations

Application to the CARMENES radial-velocity survey

A. Garcia-Piquer¹, J. C. Morales^{1,2}, I. Ribas¹, J. Colomé¹, J. Guàrdia¹, M. Perger¹, J. A. Caballero^{3,4}, M. Cortés-Contreras⁵, S. V. Jeffers⁶, A. Reiners⁶, P. J. Amado⁷, A. Quirrenbach³, and W. Seifert³

¹Institut de Ciències de l'Espai (IEEC-CSIC), Campus UAB, C/Can Magrans s/n, 08193 Bellaterra, Spain, e-mail: agarcia@ice.csic.es

²LESIA-Observatoire de Paris, CNRS, UPMC Univ. Paris 06, Univ. Paris-Diderot, 5 Pl. Jules Janssen, 92195 Meudon CEDEX, France

³Landessternwarte, Zentrum für Astronomie der Universität Heidelberg, Königstuhl 12, 69117 Heidelberg, Germany

⁴Centro de Astrobiología (CSIC-INTA), Camino Bajo del Castillo, 28691 Villanueva de la Cañada, Madrid, Spain

⁵Departamento de Astrofísica y Ciencias de la Atmósfera, Facultad de Ciencias Físicas, Universidad Complutense, 28040 Madrid, Spain

⁶Institut für Astrophysik, Friedrich-Hund-Platz 1, 37077 Göttingen, Germany

⁷Instituto de Astrofísica de Andalucía (CSIC), Glorieta de la Astronomía s/n, 18008 Granada, Spain

May 27, 2022

Abstract

Targeted spectroscopic exoplanet surveys face the challenge of maximizing their planet detection rates by means of careful planning. The number of possible observation combinations for a large exoplanet survey, i.e., the sequence of observations night after night, both in total time and amount of targets, is enormous. Sophisticated scheduling tools and the improved understanding of the exoplanet population are employed to investigate an efficient and optimal way to plan the execution of observations. This is applied to the CARMENES instrument, which is an optical and infrared high-resolution spectrograph that has started a survey of about 300 M-dwarf stars in search for terrestrial exoplanets. We use evolutionary computation techniques to create an automatic scheduler that minimizes the idle periods of the telescope and that distributes the observations among all the targets using configurable criteria. We simulate the case of the CARMENES survey with a realistic sample of targets, and we estimate the efficiency of the planning tool both in terms of telescope operations and planet detection. Our scheduling simulations produce plans that use about 99% of the available telescope time (including overheads) and optimally distribute the observations among the different targets. Under such conditions, and using current planet statistics, the optimized plan using this tool should allow the CARMENES survey to discover about 65% of the planets with radial-velocity semi-amplitudes greater than 1 m s^{-1} when considering only photon noise. The simulations using our scheduling tool show that it is possible to optimize the survey planning by minimizing idle instrument periods and fulfilling the science objectives in an efficient manner to maximize the scientific return.

Keywords: Astronomical instrumentation, methods and techniques, Methods: miscellaneous, Surveys, Planetary systems, Stars: late-type

1 Introduction

Radial-velocity surveys, together with dedicated photometric space missions such as *CoRoT* and *Kepler*, have proved to be the most efficient way of discovering exoplanets. Radial-velocity surveys have generally been focused on solar-type stars, but recently the interest in planets orbiting late-type stars has increased. Due to their lower mass, the radial-velocity semi-amplitude induced by rocky planets around M dwarfs is 1.5–5 times larger than in the case of solar-type stars for similar orbital periods. This makes low-mass stars uniquely suited to the detection of Earth-like planets provided that instruments reaching the 1 m s^{-1} precision level are available. Particularly interesting are rocky planets in the habitable zones of their host stars, whose radial-velocity signals can reach a few m s^{-1} in the case of M dwarfs. However, a spectroscopic survey of low-mass stars has to face two main challenges: 1) the targets are generally faint and 2) they show higher levels of intrinsic variability due to higher stellar magnetic activity than Sun-like stars. For this reason, less than 100 exoplanets

out of the over 3500 known to date have been discovered orbiting M dwarfs [e.g., Bonfils et al., 2013; Delfosse et al., 2013; Tuomi et al., 2014; Astudillo-Defru et al., 2015], and most of them are around early-M dwarfs.

CARMENES¹ (*Calar Alto high-Resolution search for M dwarfs with Exo-earths with Near-infrared and optical Échelle Spectrographs*) is a next-generation instrument aiming at the discovery and study of a statistically significant sample of exoplanets around M dwarfs using precise radial velocities. CARMENES is mounted on the 3.5-m Zeiss telescope at the Calar Alto Observatory [Almería, Spain; Sánchez et al., 2007, 2008], and it has been built by a German-Spanish consortium [Quirrenbach et al., 2014]. It consists of two spectrographs, one sensitive to visible light and another one to the near infrared. The radial velocity precision is expected to be of the order of 1 m s^{-1} , similar to current instruments in the visible, such as HARPS [Mayor et al., 2003] and HARPS-North [Cosentino et al., 2012]. However, the main advantage of CARMENES is the simultaneous measurement of Doppler shifts over a very wide spectral range from the visible ($>0.52 \mu\text{m}$) to the near infrared ($<1.71 \mu\text{m}$). The infrared channel is designed to monitor the radial velocity of stars in the wavelength region of the spectra where late-type dwarfs emit the bulk of their light. On the

¹<http://carmenes.caha.es>

other hand, the visible channel has as well plenty of radial velocity information (spectral lines are abundant), and the combination with infrared measurements is ideal to monitor stellar activity, thus providing means of disentangling true exoplanet signals from other effects [Reiners et al., 2010, 2013]. As part of the guaranteed-time observations (GTO), CARMENES is surveying about 300 M dwarfs [Caballero et al., 2013; Alonso-Floriano et al., 2015]. The commissioning of the instrument ended in December 2015 and regular operations started in January 2016. The GTO survey will extend for at least three years, using over 600 nights of telescope time, with the goal of discovering dozens of new planets, particularly focusing on those residing in the habitable zones of their stars.

One of the major challenges of the CARMENES survey is the efficient planning of the observations of the numerous targets in the sample. In general, any kind of astronomical survey requires the execution of a large number of observations fulfilling several constraints. Some of these constraints can be predicted (e.g., visibility and elevation of the object) and have to be necessarily satisfied, and others are unknown until the time of execution of the observations (e.g., integration time, environmental conditions). In addition, there are some scientific constraints that should be optimized, such as the number of targets that have to be observed and the number of observations of each target [Perger et al., 2017]. The optimization of these constraints is a key factor for obtaining a suitable schedule with an adequate exploitation of the resources and with a high scientific return. Due to the large number of parameters involved, the planning and scheduling of observations carried out by human operators is a laborious and complicated process that does not guarantee an optimal result.

The CARMENES GTO survey also includes a careful planning of the observations to ensure the most efficient use of the telescope time and thus to maximize the science output. Although most past surveys have used a manual approach to planning, new projects increasingly appreciate the importance of carefully optimizing the observation schedule. In this sense, different mathematical tools to solve automated planning and scheduling problems have been developed, ranging from simple heuristics to more complex Artificial Intelligence applications [Donati et al., 2012; Kitching & Policella, 2013]. Examples include the scheduling tools of ALMA [Espada et al., 2014], Las Cumbres Observatory Global Telescope [Brown et al., 2013], *EChO* [Garcia-Piquer et al., 2014c], the Automated Planet Finder Telescope [Burt et al., 2015], MrSPOCK for the *Mars Express* mission [Cesta et al., 2009], the *James Webb Space Telescope* [Giuliano et al., 2011], and the SOFIA mission [Civeit, 2013]. To complement these examples, a summary of other planning and scheduling tools used in astronomical observatories can be found in [Colomé et al., 2012].

In particular, Genetic Algorithms (hereafter GAs), which are Evolutionary Computation (EC) techniques [Holland, 1975], are very useful for this purpose. EC is an Artificial Intelligence subfield focused on emulating natural evolution by means of combining potential solutions using selection, combination and mutation operators [Freitas, 2002]. The goal of GAs is to efficiently explore a large amount of potential solutions in order to find near-optimal solutions [Goldberg, 1989] fulfilling

all constraints and optimizing the goals defined in the problem. GAs must be adapted to the particularities of the problem in order to obtain suitable results [Garcia-Piquer et al., 2014a]. Generally, a scheduler for astronomical observations has more than one parameter that needs to be optimized, resulting in a Multi-objective Optimization Problem (MOP) that can be defined as the problem of finding a vector of decision variables satisfying constraints and optimizing a vector function whose elements represent the objective functions [Osyczka, 1985]. These functions form a mathematical description of performance criteria that are usually not disjoint (i.e., they are in conflict with each other). Hence, the term “optimize” refers to finding a solution that yields acceptable values for all objective functions [Coello Coello, 1999]. Usually there is not a single point that simultaneously optimizes all the objective functions of a MOP. Therefore, in these problems it is necessary to look for trade-offs, rather than single solutions. The concept of Pareto Optimality [Pareto, 1897] defines that we can consider a Pareto optimal when no feasible vector of decision variables exists that would decrease some criterion without causing a simultaneous increase in at least one other criterion. Thus, this concept almost always does not yield a single solution but a set of solutions called the Pareto optimal set. All solutions included in the Pareto optimal set are non-dominated (i.e., there is no solution better than the rest) and they have a different trade-off between objectives [Garcia-Piquer, 2012]. The plot of the objective functions whose non-dominated vectors are in the Pareto optimal set is called the Pareto front [see, Coello Coello, 1999, 2001, for further details]. Multi-Objective Evolutionary Algorithms [hereafter, MOEAs Coello Coello et al., 2007] are recognized as one of the most valuable and promising approaches to addressing complex and diverse problems of multi-objective optimization.

In this paper we present in detail the scheduling tool developed in the context of the CARMENES GTO survey, already introduced in [Garcia-Piquer et al., 2014b]. Although it has been designed for a radial-velocity application, it is seamlessly adaptable to other purposes and constraints [see e.g., Garcia-Piquer et al., 2014c]. In Sect. 2 we describe the general implementation of the scheduling tool, based on GAs. In Sect. 3 we apply the constraints of the CARMENES survey and we analyze the efficiency of the scheduling algorithms in terms of telescope and instrument operations. Finally, in Sect. 5 we analyze the results of the optimal schedule calculations to assess their scientific efficiency in the case of a radial velocity survey and to estimate the CARMENES expected exoplanet yield. The conclusions are presented in Sect. 6.

2 CAST

The first step to schedule an astronomical survey is the preparation of the sample of targets and the identification of observational constraints that may be defined by the target stars, the telescope and instrument design, and the science requirements. As mentioned above, CARMENES will carry out a survey of ~ 300 M dwarfs for a period of at least three years. For this paper, we have used a list of 309 high-priority po-

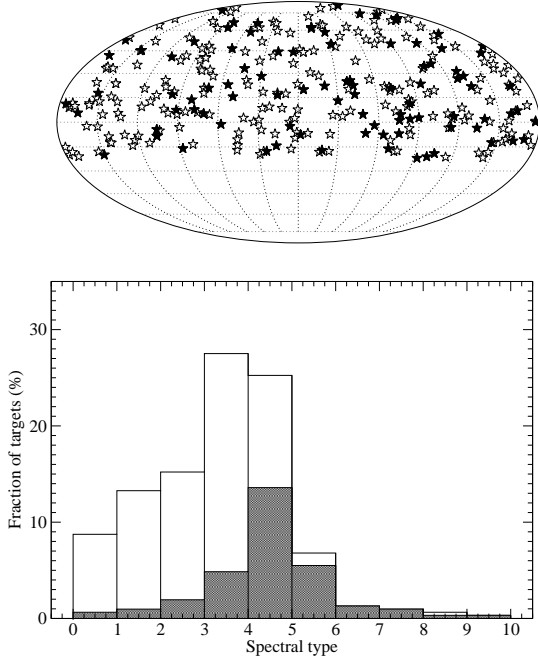


Figure 1: *Top:* Mollweide projection of the distribution on the sky of the 309 CARMENES targets used in our simulations. *Bottom:* Spectral type distribution of the targets. In both panels, filled symbols and bars indicate active stars with the $H\alpha$ line in emission.

tential target candidates compiled in the CARMENES input catalogue [dubbed Carmencita; Caballero et al., 2013; Alonso-Floriano et al., 2015]. The CARMENES science objectives for at least 60 observations to be obtained for each target. These high-priority M dwarfs are selected from a larger sample by removing unsuitable systems for the survey (e.g., faint stars in the J -band for their spectral subtypes, or spectroscopic or close visual binaries). The list comprises targets distributed among all M dwarf spectral subtypes as shown in Fig. 1, which also depicts the distribution of targets on the sky. The J magnitude ranges from 4.2 to 11.2 mag, with a mean value of 7.7 ± 1.0 mag. For simplicity, the simulation experiments presented in this paper assume that all targets have the same priority. However, an external priority value is included in the description of the algorithm. This is because such functionality has been implemented in the operational CARMENES scheduler in case that it needs to be considered for the optimization over the course of the survey (e.g., to increase measurement cadence of interesting targets or to sample specific periods). This priority is an integer value that is assigned to each target by a user, with larger values indicating higher priority.

Regarding the constraints of the survey, they can be divided into two different categories: hard constraints and soft con-

Table 1: List of CARMENES observational constraints.

Constraint	Category	Computation
Night	Hard	In advance
Elevation	Hard	In advance
Moon influence	Hard	In advance
Visibility duration	Hard	In advance
Pointing	Hard	In advance
Overlapping	Hard	In advance
Overhead time	Hard	In advance
Environmental conditions	Hard	On the fly
Observing time	Soft	In advance
		On the fly
Observation deviation	Soft	In advance
Observing cadence	Soft	In advance

straints. The first ones have to be necessarily satisfied, and the second ones express a preference of some target combinations over others. Thus, the final scheduling solution must fulfill all hard constraints and should optimize soft constraints.

2.1 Scheduling constraints

In the case of the CARMENES GTO survey, the hard constraints implemented in the CARMENES Scheduling Tool (hereafter CAST) are mainly related to the visibility of the targets from the Calar Alto Observatory, the operation overhead times, and the environmental conditions. These restrictions can also be adapted for other surveys and facilities such as space-based telescopes [see e.g., Garcia-Piquer et al., 2014c]. The *hard constraints* identified are summarized in Table 1 and are described as follows:

1. *Night.* The object shall only be observed from afternoon twilight to morning twilight. The coordinates of the targets on the sky and twilight times are computed according to the date of observation and the location of the observatory. Additionally, if needed, the observability window of each target can be computed according to given ephemerides for the case of objects with periodic variability. For this paper we have considered the start of the astronomical twilight at Calar Alto Observatory as a conservative approach (Sun at -12 deg elevation).
2. *Elevation.* The elevation of each object is calculated according to its equatorial coordinates and the geographic coordinates of the observatory. The objects shall only be observed if they exceed a specific elevation for at least a certain amount of time. The elevation and time are two parameters that can be introduced in the global configuration of CAST. For CARMENES, the scheduling requirement is that a target must be above 30 deg for a time span longer than its estimated integration time.
3. *Moon influence.* Targets shall be observed when 1) the Moon is below the horizon or 2) the Moon is sufficiently far so that the observation is not significantly contaminated by background light. We have established that the minimum acceptable distance to the Moon (r_{\min}) is 20 deg. Beyond this distance, a hard constraint function on the Moon is evaluated to select only targets that are

at least 5 magnitudes brighter than the background (see Appendix A.1 for further details).

4. *Visibility duration.* The total time during which the *Night*, *Elevation* and *Moon influence* constraints are fulfilled shall be equal or higher than the minimum visibility time required for a target observation. This minimum time corresponds to the exposure time, which is computed using a calibration as a function of *J*-band magnitude using real CARMENES observations (see Appendix A.2 for more details). The maximum exposure time is set to 30 minutes to avoid biasing the barycentric correction. This exposure time limitation only affects 35 late-type dwarfs in our sample, which would need longer integration times according to their *J*-band magnitude. However, the effect of the reduction of exposure time is counterbalanced by the fact that for faint targets, typically late M-dwarf stars, the radial-velocity precision needed to detect planets is not as high as for earlier types.
5. *Pointing.* In case of pointing restrictions, targets shall only be observed if they are between minimum and maximum elevations as defined by the survey requirements. Moreover, in the case of CARMENES, the telescope dome has a “segmented” hatch that allows five open window configurations with different apertures (see Appendix A.3 for more details). If the window configuration needs to be changed (because of vignetting) during target integration, the slide would temporarily block the telescope aperture and the observation will be affected. Thus, an observation shall only be selected if the target can be observed without being obstructed for the entire duration of the estimated integration time.
6. *Overlapping.* In operational terms, there are three kinds of tasks to be considered: 1) target observation, 2) read-out of the previous observation, and 3) slewing to acquiring a new target. Only tasks 2) and 3) can be executed in parallel.
7. *Overhead time.* Pointing to a particular object requires a specific telescope and instrument configuration. The time between consecutive observations considers both the telescope slew & acquisition time and the instrument read-out time. The former includes the time needed to move the dome, the hatch and the telescope, and an overhead slew time for acquisition, while the latter is defined by the detector properties. We assume the total overhead time between observations to be the duration of the process that takes a longer time (see Appendix A.4 for the detailed logical operations). For the CARMENES scheduler, we assume a telescope and dome slew rate of 1 deg per second, and 60 s to change the dome hatch (the segments can be moved together, so the time overhead is independent of the number of segments to move). The overhead slew time is 120 s and the detectors read out time is less than 40 s.
8. *Environmental conditions.* An observation can be programmed when the environmental conditions permit. In

operation mode during the survey, the CARMENES Instrument Control System [Garcia-Piquer et al., 2014b] informs CAST if the environmental conditions are suitable for observation. In the simulation mode presented here, we have used a weather model based on Calar Alto environmental conditions from 2004 to 2006 (Calar Alto Observatory, priv. comm.), thus taking into account seasonal weather influence. We assumed that the dome is closed if: 1) relative humidity reaches 98 %, and must be closed until it is equal to or below 95 % for at least 20 minutes; 2) the outside temperature is below -15°C ; or 3) the wind speed is above 24 m s^{-1} . Furthermore, to be conservative, we assume that a given night has a maximum probability of 20 % of cloudiness in low humidity conditions or of technical issues impeding observations. And, finally, the simulator increases the integration time randomly up to 20 % to simulate the effect of high clouds.

On the other hand, in terms of scheduling, science requirements are identified as *soft constraints*. These restrictions are also summarized in Table 1 and include:

1. *Observing time.* The integrated global observing time (i.e., the time that the telescope is observing), especially that of high-priority objects, should be maximized. This guarantees that the most interesting targets are sufficiently observed.
2. *Observation deviation.* The variance of the number of times that objects of the same priority have been observed in the complete survey should be minimized. This constraint should ensure that all targets will have a proper share of assigned observing time.
3. *Observing cadence.* It is possible to select the number of observations per night required for each target. As an optional constraint, the planning tool includes functionality to observe the targets at appropriate times to increase planet detectability by, e.g., averaging the intrinsic stellar noise on radial velocities [see, e.g., Dumusque et al., 2011a,b] or by optimizing the periodogram window function over a certain orbital period interval (i.e., avoiding peaks or gaps). In case of transient objects, target ephemerides are considered. For the present work, we assume that each target will be observed no more than once per night and randomly for the duration of the survey.

Some of the constraints can be computed in advance but others, such as weather conditions (environmental conditions), can only be determined in real time during observations and the scheduler must be reactive to their variations. For this reason, although being an independent system, CAST is connected with the Instrument Control System from which it receives environment parameters and return an observation request optimized according to current conditions. In order to reduce waiting times, one of the CAST requirements is that it should invest less than five seconds in selecting the next target to be observed. The simultaneous fulfilment of the hard constraints and the optimization of the soft constraints should provide a scheduling solution that maximizes the scientific return of the survey.

Table 2: Constraints used by the CAST Long-, Mid-, and Short-term schedulers.

Constraint	Long-term	Mid-term	Short-term
Hard constraints			
Night	✓	✓	✓
Elevation	✓	✓	✓
Moon influence	✓	✓	✓
Visibility duration	✓	✓	✓
Pointing	✓	✓	✓
Overlapping		✓	✓
Overhead time		✓	✓
Environmental conditions			✓
Soft constraints			
Observing time		✓	✓
Observation deviation		✓	✓
Observing cadence	✓		

2.2 Scheduling optimization

Given the large number of targets of the CARMENES sample and its conditions, the complexity in computing the enormous amount of possible combinations in search for a near-optimal scheduling solution is unaffordable for human operators. Hence, the scheduling of CARMENES observations can be addressed as a constraint-satisfaction problem, which is a combinatorial problem that seeks an assignment of values to its variables that will satisfy all given constraints. The algorithms used to find the optimal solution to these kind of problems require a computation time that grows exponentially with the size of the input. Consequently, approximate or heuristic methods are useful to find feasible solutions, or those that satisfy most of the constraints, in a reasonable computation time [Nonobe & Ibaraki, 1998]. In CAST, GA techniques are implemented in order to efficiently explore the large amount of potential combinations of observations with the goal of selecting those that are more efficient.

The algorithms of CAST were presented in [Garcia-Piquer et al., 2014b] but we provide the basic details here. Two scheduling strategies are included in CAST: off-line and on-line [Rasconi et al., 2006b]. The off-line strategy includes two planning tools, Long-term and Mid-term schedulers, which are designed to plan the targets to be observed within a time interval according to the hard constraints that can be predicted. The on-line strategy considers a Short-term scheduler that takes into account all constraints and adapts the previously computed mid-term plan to the immediate circumstances [Rasconi et al., 2006a]. Table 2 summarizes the constraints considered by each of the three schedulers. Their combination is illustrated in Fig. 2 and we provide additional details on the three scheduling tools in Sect. 2.3.

2.3 Genetic Algorithm for the off-line strategy

The Long-term and the Mid-term schedulers use a MOEA to plan the science observations by promoting the soft constraints defined for each scheduler. The MOEA process, as a GA,

is generally based on selection, reproduction, and mutation processes. This paradigm makes it possible to explore all regions of the parameter space, which is a vast area with a large amount of potential solutions, in search of the best solutions. This kind of algorithms begins with a set of initial solutions that are improved through an iterative cycle based on evaluating, selecting, recombining, and mutating them. The key aspect for finding high quality solutions lies in the definition and design of individual representation, the genetic operators, and the objectives to be optimized [Goldberg, 2002; Garcia-Piquer, 2012]. For more details about the design of a MOEA, the reader is referred to Appendix B. The MOEA applied is based on the NSGA-II procedure [Deb et al., 2002], which is one of the most well-known MOEAs. However, with the aim of obtaining a suitable optimization solution, it is necessary to design ad hoc parts of the algorithm according to the problems to be solved, so the Long-term and Mid-term schedulers have some differences.

2.3.1 Long-term scheduler

The Long-term scheduler plans object observations with a time scope of several months. It takes into account the *Night*, *Elevation*, *Moon influence* and *Visibility duration* constraints. A procedure based on MOEAs is applied to identify the best nights when each object should be observed by optimizing the soft constraint regarding the *Observing cadence* constraint. The resulting plan provides a list of potential observation dates for each object assuming that all scheduled nights for the survey are suitable. Besides, the Long-term scheduler is run periodically to take into account observations previously done, thus counteracting any effect that unpredicted bad weather may have on the optimization. The execution of this scheduler is not time-critical because it is run daily before the start of telescope operations and without interaction with the Instrument Control System to retrieve weather information. Therefore, it can be used as a standalone planning tool for any observatory.

The design of the MOEA used in the Long-term scheduler is defined as follows:

- The individual genotype uses a binary encoding that represents if the target is planned on a given night. Each individual consists of \bar{N} genes $\{o_1, \dots, o_{\bar{N}}\}$, where \bar{N} is the cardinality of the set of nights (N) that the Long-term scheduler considers (e.g., the number of nights in three months) and o_i corresponds to night i . Moreover, the o_i value has to be 0 or 1, where 0 indicates that the target is not planned in the corresponding night and 1 indicates that the target is planned. The order of the targets in the genotype indicates a temporal sequence from the first night considered to the last one. The initial population is built by creating N_I new individuals assigning to each allele a value of 0 or 1 with a probability of 0.5. This representation does not allow unfeasible individuals.
- The selection, crossover and mutation operators are described in Appendix B.2. In the case of the Long-term scheduler, a mutated gene g' is obtained by negating g

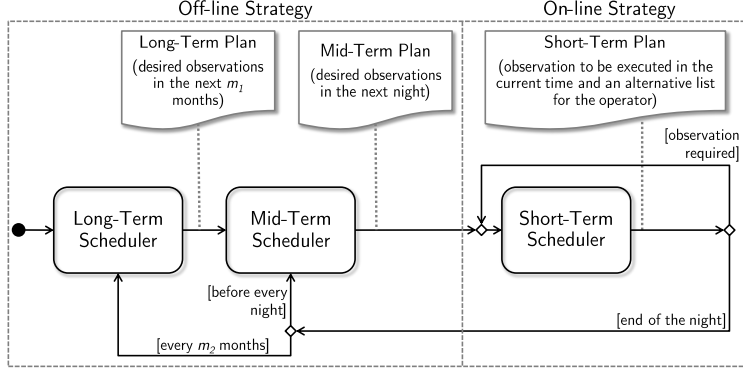


Figure 2: Combination of the three schedulers of CAST. The Long-term scheduler plans observations with a time scope of several months (m_1) and is recomputed after a specific number of months (m_2). The Mid-term scheduler is executed daily and computes the observations to be performed during each night. The Short-term scheduler is executed during the night after every exposure and computes the next optimal observation and an alternative ranked list of alternatives. In this work, we set $m_1=6$ and $m_2=3$ months.

(i.e., alleles that are 0 become 1, and those that are 1 become 0).

- The Long-term scheduler has the optimization goal of identifying the nights when an object should be observed according to the *Observing cadence* constraint. In the case of CARMENES, it is desirable to observe the targets when they are near their culmination. The optimization objectives promote the observation of an object near meridian crossing at the same time that maximizes the number of observations done. Thus, two objective functions are defined: F_c promotes the observations of an object near meridian crossing and F_n promotes the number of observations of the object, as described by Eqs. 1 and 2, respectively. Where O is the set of nights when target t is observed, N is the set of genes of the individual chromosome (i.e., the number of nights to be planned), $Z_{\min}(t)$ computes the minimum zenith angle that target t can achieve, $Z_{\min}(t, n)$ computes the minimum zenith angle that target t can achieve in night n , and \overline{O} and \overline{N} are the numbers of elements (cardinality) in sets O and N , respectively (i.e., the number of nights when a target is observed and the total number of nights in the planning). F_c and F_n have normalized values between 0 and 1, and they are optimized when minimized.

$$F_c(O, t) = 1 - \frac{1}{\overline{O}} \cdot \left(\sum_{o \in O} \frac{Z_{\min}(t)}{Z_{\min}(t, o)} \right). \quad (1)$$

$$F_n(N, O) = 1 - \left(\frac{\overline{O}}{\overline{N}} \right). \quad (2)$$

- We consider that the most suitable solution is the individual that has the lower average of objectives (the defined objectives have to be minimized to be optimized) from all the individuals in the first Pareto front (i.e., non-dominated individuals).

2.3.2 Mid-term scheduler

The Mid-term scheduler plans the observations that should be executed during a specific night by optimizing the *Observing time* and *Observation deviation* soft constraints, and according to the results of the long-term plan. Moreover, the resulting mid-term plan fulfills all the hard constraints that are predictable: *Night*, *Elevation*, *Moon influence*, *Visibility duration*, *Pointing*, *Overlapping*, and *Overhead time*. The execution of this scheduler is not time critical because it can be run before the start of the nightly telescope operation, and therefore, a GA is used to obtain a near-optimal plan.

The MOEA used in the Mid-term scheduler is designed as follows:

- The proposed individual genotype is made up of double numbers that represent the starting time of the observation of the targets. Each individual consists of \overline{T} genes $\{o_1, \dots, o_{\overline{T}}\}$, where \overline{T} is the cardinality of the set of targets to be planned (T), and o_i corresponds to target i . Moreover, the o_i value has to be between the range $[w_{st}, w_{et} - d_t]$, where w is a random uniform window in W_t , which are all the visibility windows in the night for target t , w_{st} is the Julian day of the starting time of window w for target t , w_{et} is the Julian day of the ending time of window w for target t , and d_t is the estimated integration time in Julian days for target t (see Appendix A.2). Moreover, o_i can have a value of -1 indicating that target i does not have a starting time assigned (i.e., it is not planned). The order of the targets in the genotype does not indicate a temporal sequence, but it is only the order of the targets in the input data. The temporal sequence of targets is defined by the alleles, because they indicate the starting time assigned to each target. For instance, a target in position i of the genotype can be planned in a time window previous to the time window of target $i - 1$. The initial population is built by creating N_I new indi-

viduals assigning to each allele o_i a -1 value or a value in the range between $[w_{st}, w_{et} - d_t]$ following a uniform distribution. The process to build each individual is based on placing the observations of the targets, selected in random order, and avoiding overlaps. In case of overlapping, the target is unplanned (i.e., a value -1 is assigned).

- Selection, crossover and mutation operators work as Appendix B.2 shows. In the Mid-term scheduler, the mutation operator alters a gene g' by changing its allele with a value inside the potential time windows of the corresponding target. Thus, a mutated gene g' changes its allele with a random uniform value μ in the range $[w_{st}, w_{et} - d_t]$ and -1 (i.e., $g' = \mu$). In this case, the crossover of two feasible individuals can generate unfeasible offspring due to overlapping, and the mutation of a feasible individual can also generate an unfeasible solution. This is solved by a repairing procedure devoted to obtain feasible new individuals, as the next point explains.
- An individual represents the time windows assigned to target observations, but it does not consider the slew time between two observations. Thus, this aspect has to be considered for obtaining the final planning codified by each individual. This modification can produce an unfeasible individual because it can have conflicting observations (i.e., presence of overlaps in the observations). There are two ways for obtaining an unfeasible individual that requires repair during the GA process: 1) the individual has overlapping between two or more observations, and 2) there is overlapping between two or more observations when slew time is added to each observation. We may find that it is necessary to repair the individuals after the mutation process in order to obtain feasible ones. Thus, the main idea of the repair operator is to solve all overlaps in the individual by unplanning conflicting targets. The unplanning of one target can solve overlaps between several targets.
- The optimization goal of the Mid-term scheduler is to plan the selected objects according to two objectives related to the *Observing time* and *Observation deviation* soft constraints, with the aim of minimizing the instrument idle time (time of the night during which the instrument is not acquiring scientific data) weighted with the priority completeness of the targets, and mitigating the problem of scheduling the objects that require longer observations. Consequently, the Mid-term scheduler optimizes two functions. F_w promotes the time scheduled for observations of objects near meridian crossing according also to their priority, and F_d promotes a proper distribution of the observations of the objects with the same priority, as described in Eqs. 3 and 4, respectively. Where S is the set that contains the observations scheduled in the night, o_{target} is a target associated to observation o , o_{datetime} is the mid time of observation o , $\text{integrationTime}(o_{\text{target}})$ computes the estimated integration time in seconds of a target observation, nightduration indicates the duration of the night in seconds, $\text{priority}(o_{\text{target}})$ is the priority of the target

associated to observation o normalized according to the priorities of all targets, $Z_{\min}(o_{\text{target}})$ computes the minimum zenith angle that target o_{target} can achieve during the night, $Z_{\min}(o_{\text{target}}, o_{\text{datetime}})$ computes the minimum zenith angle of target o_{target} at the date and time o_{datetime} , P is the set of priorities, S_p is the set that contains the observations of targets with priority p in the night, T_p is the set of the targets with priority p , S_t is the set that contains the observations of target t , and \overline{P} , \overline{S}_p , \overline{T}_p , \overline{S}_t are the number of elements (cardinality) in sets P , S_p , T_p , and S_t , respectively. F_w and F_d have values between 0 and 1, and they are optimized when minimized.

$$F_w(S) = 1 - \left(\frac{\sum_{o \in S} (\text{integrationTime}(o_{\text{target}}) \cdot \text{weight}(o))}{\text{night duration}} \right),$$

$$\text{weight}(o) = \text{priority}(o_{\text{target}}) \cdot \frac{Z_{\min}(o_{\text{target}})}{Z_{\min}(o_{\text{target}}, o_{\text{datetime}})}. \quad (3)$$

$$F_d(S) = \frac{\sum_{p \in P} \text{stdev}(S, p, \overline{p})}{\overline{P}},$$

$$\overline{p} = \frac{\overline{S}_p}{\overline{T}_p}, \quad (4)$$

$$\text{stdev}(S_p, p, \overline{p}) = \sqrt{\frac{\sum_{t \in T_p} (\overline{S}_t - \overline{p})^2}{\overline{T}_p - 1}}.$$

- The same strategy as in the Long-term scheduler is applied to select the most suitable solution (see Sect. 2.3.1).

2.3.3 Short-term scheduler

The Short-term scheduler computes the next observation to be executed during the night by optimizing the *Observing time* and *Observation deviation* soft constraints and by considering all previous observations. Moreover, the selected observation fulfills all the hard constraints, Thus, this scheduler reacts to immediate conditions (weather, errors, delays, events). Unlike the Long-term and Mid-term schedulers, the Short-term scheduler is time critical because it has to select an observation in a short time. For this reason, in order to avoid intensive calculations, it repairs the night schedule obtained by the Mid-term scheduler [Akturk & Kılıç, 1999] using astronomy-based heuristics [Giuliano et al., 2007] instead of using a GA. The Short-term algorithm is called after the end of an observation, and its process is explained below.

First, the algorithm removes all objects whose assigned observation period ended before the current time from the mid-term plan and selects the next target. For this target, the code computes the slew time of the telescope. The target observation obtained for the mid-term plan is adapted (i.e., advanced or delayed) according to the current time, computed slew time, and integration time. This observation is only selected if it fulfills the hard constraint requirements until the end of the observation. Otherwise, it is discarded and the gap between the current time and the start of the next observation in the

mid-term plan is filled. The filling process sorts all the observations that (1) are not already in the mid-term plan, (2) fulfill the hard-constraints during the entire window, and (3) can be completed in the available time. This ranking is done according to several criteria described below. Finally, the first observation in the sorted list is selected as the next observation. The filling process is repeated until the gap is filled or there are not target observations left. Each target selected by the Short-term scheduler is sent to the Instrument Control System, and the information on the success of the observation is stored in the database for use in subsequent scheduler runs. Besides, the sorted list of objects can be provided to the operator for override in case of need. Fig. 3 shows an example of the most common situation where the Short-term scheduler needs to repair the mid-term plan to select the next target to be observed.

The ranking of the targets is key in the process of repairing the mid-term plan by filling a gap between the last executed observation and the next observations recommended by the mid-term plan. This ranking is based on astronomical heuristics, and the targets are sorted according to the first rule, then the second rule, and so on. The defined rules are:

1. The number of times that the target is observed during the current night (smallest to largest).
2. The target is not in the remaining mid-term plan.
3. The priority of the target (largest to smallest).
4. The number of times that the target has been observed in the survey (smallest to largest).
5. The proximity to meridian crossing according to Eq. 3 (largest to smallest).

The main idea of this process is to fill the gaps with interesting objects at the current time, according to the times that they have been observed, their priority, and the proximity to meridian crossing. Rule 2 is key to fill gaps without affecting excessively the mid-term plan, which has been globally optimized.

3 CAST scheduling efficiency

In general, CAST is focused on optimizing the three soft constraints described in Sect. 2: observing time, observation deviation and observation sequence. The first two constraints maximize the use of the telescope and the instrument while the last one is included as an optional condition to increase the scientific return.

In this section we run a set of simulations of the CARMENES survey with the aim of analysing the efficiency of CAST in the use of resources. For a quantitative analysis, we have defined different metrics related to the use of the telescope and the instrument. In particular, we have computed the fraction of targets that are planned by the scheduler, the total number of observations, the fraction of available time that the telescope is operating, the fraction of time during which the instrument is performing science observations, and the fraction of overhead time. In Sect. 5 we describe the impact of

the observing plans optimized by CAST on the CARMENES scientific results.

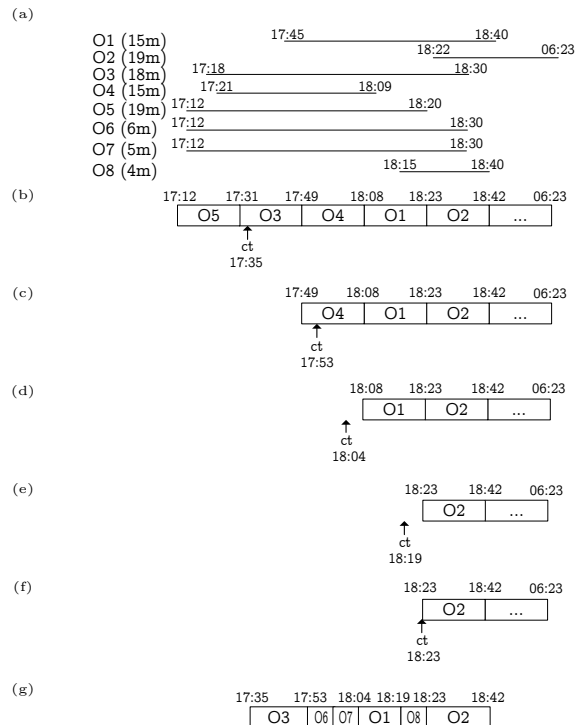


Figure 3: Examples of observation selection corresponding to time ct . O_t indicates an observation of target t . For simplicity, the slew time between observations is not considered. (a) represents the visibility (i.e., fulfillment of the hard constraints) and integration time of each target in minutes. The line indicates the time window where the target is visible, and the integration time of the observations in minutes is indicated in parentheses. (b), (c), (d), (e), and (f) present the objects planned in the mid-term plan that are available at ct . (b), shows how the Short-term scheduler discards $O5$ because it is not active in the mid-term plan at ct . Thereafter, $O3$ will be shifted and will start at 17:35, because the observation will end inside its visibility period as it is visible until 18:30. Next, in (c), $O4$ is not visible after 18:09 and it cannot be completed if it is delayed until 17:53. Thus, $O4$ is removed from mid-term plan. Consequently, there is a gap between 17:53 and 18:08 that will be filled with one or several new observations. In this case, we assume that two new observations are executed ($O6$, $O7$). (d) depicts how the gap is only filled until 18:04 because no visible target that is not already in the mid-term plan fits in the remaining window. $O1$ is advanced and it will start at 18:04 because it is visible at this time. In (e), $O2$ is not visible until 18:22, so it cannot be advanced. The gap between 18:19 and 18:23 will be filled with one or several new observations. In this case, we assume that one new observation is executed ($O8$). Finally, in (f), $O2$ can start at the time scheduled by the mid-term plan. (g) shows the observations executed by the Short-term scheduler according to the process described.

Table 3: Genetic algorithm parameter configuration.

Parameter	Value
Long-term generations	1000
Mid-term generations	1000
N_I	50
N_P	100
p_s	0.4
p_c	0.9
p_μ	$1/\bar{l}$

3.1 CARMENES configuration

To be as close as possible to the real survey, we have adopted the following procedure to run CAST. The Long-term scheduler has a scope of six months, and is executed every three months during the survey. The Mid-term scheduler is executed every day taking into account the observations acquired during the previous night. The Short-term scheduler is executed “on the fly” each time a new observation is required and takes into account the mid-term plan, the observations already carried out during the night, and any variation on the weather or instrument conditions.

In terms of parametrization, the Long-term and Mid-term schedulers have several parameters related to the GA as explained before. Table 3 summarizes the parameter configuration used in the experiments done, which are related to the number of generations of the evolutionary algorithm, the number of elements in the initial set of solutions and in the subsequent generations and the probabilities of selection, crossing, and mutation.

3.2 Results

Because GAs are stochastic methods, CAST is executed 50 times with different random seeds with the aim of avoiding any bias in the results due to convergence to local minima. Hereafter, each of these executions is referred to as a trial. Table 4 summarizes the parameters of the simulations and the results of the metrics used to evaluate the efficiency of CAST.

From the the simulated weather statistics, the average usable time for observations at Calar Alto is around 60% of the total night time. Observatory statistics actually indicate that $\sim 70\%$ of the nights are useful according to meteorological variables [Sánchez et al., 2007, 2008]. However, as explained before we have considered and additional up to 20% of lost time due to cloudiness or technical issues. Thus, in three years, there are about 6400 hours during which observations can be scheduled. The results from our simulations presented in Table 4 show that all required targets are always planned. Around 21000 observations are scheduled, occupying $\sim 99\%$ of the good weather time. The break-down of this time indicates that 84% corresponds to the telescope collecting photons and 16% is spent during slews to new positions. This means that the instrument is collecting photons during approximately 1700 hours per year. Our simulations show that CAST can optimize the observing time of the telescope

by selecting the best targets to observe according to environmental conditions at each time. In our simulations, the average integration time of the targets is around 14 minutes and we can obtain about 3.2 observations per hour of working time.

Additionally, it is important to distribute equitably the observations of all the targets. This is the second soft constraint that CAST must optimize. Fig. 4 shows the number of times that each target is observed. On average, each M dwarf in the sample is observed ~ 67 times during the three-year survey. The standard deviation of the number of observations between targets is 3, which indicates that the resources are reasonably distributed among the different targets. Only a few of them have a number of observations significantly below the average, but this is due to their very limited visibility during the year (e.g., low declination and faintness). This means that all targets will have a high number of observations and, if necessary, this number can still be increased if some of the targets are discarded during the initial sample clean-up (very fast rotators, active stars, spectroscopic binaries that passed our filters, etc.). On the other hand, the simulations with CAST could also help in the optimization of the sample since any target for which a minimum number of observations is not reached can be rejected, or upper limits to the number of observations per target can be set.

As already mentioned, CAST includes a soft constraint to define an observing scheme that maximizes planet detectability with the least number of observations. For the present work we have assumed a maximum of one observation per night for any target, but a well-sampled window function of the observations may improve the detectability of signals within a range of interesting periods. This can be quantified by computing a phase dispersion parameter given a set of previous observations for the periods of interest of each target and then estimating the next best observation that optimizes such parameter [see, e.g., Freedman et al., 1994]. These techniques to optimize the periodogram window function can only be applied once several observations per target are obtained.

3.3 Analysis of the computational performance

The computing time of the three scheduler steps with the 309 selected targets is presented in Table 5. CAST has been developed in C++ language and the experiments have been executed using only one processor of the main computer where CAST runs in Calar Alto (Dell PowerEdge R420 rack server with two Intel Xeon CPUs E5-2430 v2 with six cores at 2.50 GHz and 16 GB of RAM). The main restriction in the scheduling process is the response of the Short-term scheduler. As already explained, this is used to select the next best survey target after the end of each observation by taking into account the environmental conditions. It is required that its execution takes less than 5 seconds to prevent telescope idle time during the calculation. This requirement is fulfilled as the Short-term scheduler selects a new observation in about 56 milliseconds. The other schedulers can be executed during the day before the observations, and they do not have any time restriction. Nevertheless, they produce results in a reasonable time: about

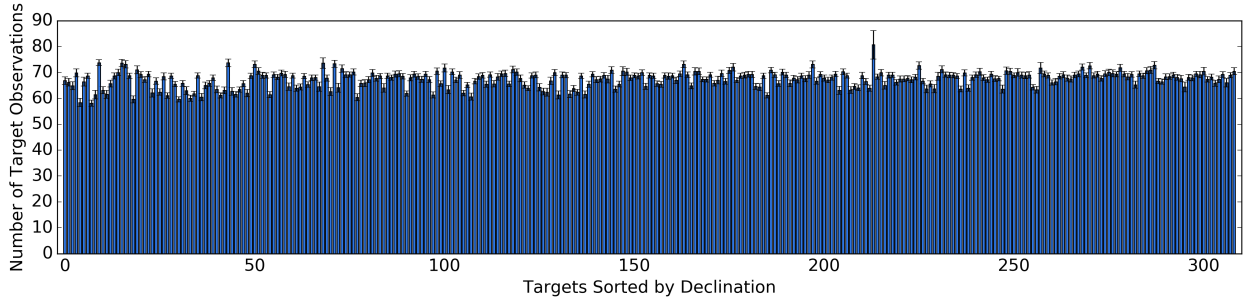


Figure 4: Number of observations scheduled for each target. The horizontal axis represents the identifier of each one of the 309 targets used in our simulations sorted by increasing declination. Declination ranges from -21 to 83 deg in our sample. The bars show the average and standard deviation values of the 50 executions.

Table 4: CAST parameters and mean values of the metrics.

CAST parameters (a)	
Days planned	1096
Total targets	309
Total observable time	10703.05 h
Unfavorable weather time	4300.23 ± 88 h
Available time for observations (b,f)	$59.82 \pm 0.82\%$ (6402.81 h)
Execution Time of CAST	23.85 ± 0.11 h
Metrics (a)	
Planned targets (c)	$100 \pm 0\%$
Observations done	20827 ± 293
Working time (d,f)	$99.05 \pm 0.06\%$ (6342.03 h)
Tracking time (e,f)	$84.18 \pm 0.03\%$ (5338.77 h)
Overhead time (e,f)	$15.82 \pm 0.03\%$ (1003.22 h)

(a)The uncertainties are computed as the standard deviation of 50 random trials.

(b)Fraction of time available for observations, excluding bad weather time.

(c)Fraction of the targets that are planned.

(d)Fraction of time with scheduled telescope operations with respect to the available time for observations.

(e)Fraction of time with respect to the working time.

(f)The number of hours is indicated in parentheses.

Table 5: Average computing times of the three scheduler strategies in the 50 trials.

Scheduler	Execution Time (s)
Long-term scheduler	1815.166
Mid-term scheduler	58.347
Short-term scheduler	0.056

30 minutes and < 1 minute for the Long-term and Mid-term schedulers, respectively.

4 CAST in real operation

CAST is in real operation since September 2016 for the CARMENES survey. The used version includes some additional functionality that is specific to the observing program and that is intended to adapt its performance to the actual working conditions. We list here some of these additional spe-

cific features that extend beyond the general design described above:

- During the survey it is possible to change the priority of an object to increase the chances of it being selected by CAST.
- It is possible to disable an object to make it unavailable for CAST.
- CAST can include the observations of telluric standard stars during the nautical twilight in the planning.
- Bright stars can also be planned during nautical twilight updating the *Night* constraint of the affected objects with the desired Sun altitude.
- A parameter is available to select the maximum number of times that a target can be observed during one night.
- It is possible to assign a cadence of observations to each target to sample different periods (from days to months).
- Interesting or standard stars can be labeled as mandatory. This implies that they must be observed every night while they have this flag active. This constraint is also considered by the Mid-term scheduler in two steps: 1) the Mid-term scheduler is executed only with the mandatory objects, following the same defined objective functions, and 2) the Mid-term scheduler is executed a second time with the remaining objects but blocking window times where the mandatory objects have been planned. The final mid-term plan is the merging of both plans.
- The quality of the night according to transparency conditions can be considered. This quality can be modified during the night by the operators. There are six keywords indicating different night quality levels: excellent, good, fair, poor, very poor and bad. When an observation is required with a night quality that is not excellent, the mid-term plan is not considered and the short-term scheduler is in charge of selecting the next observation. In this situation, the rules specified in Sect. 2.3.3 are modified as follows:

1. The proximity to meridian crossing according to Eq. 3 (largest to smallest) weighted with R_q following equation

$$R_q(t, q) = \left(\frac{t_{\text{magnitude}}}{4.2} \right)^{(q-5)}, \quad (5)$$

which relates the magnitude of an object with the quality of the night in order to increase the ranking of bright objects. In Eq. 5, $t_{\text{magnitude}}$ is the J -band magnitude of target t , and q is the quality of the night that goes from 4 (good) to 0 (bad).

2. The number of times that the target is observed in the current night (smallest to largest).
3. The priority of the target (largest to smallest).
4. The number of times that the target has been observed in the survey (smallest to largest).

5 The impact of efficient scheduling on the scientific return

5.1 Exoplanet yield simulation

In this section we analyze the impact of our scheduler algorithms in the scientific results of the CARMENES survey. We estimate how many planets would be detected in a radial-velocity survey following our planning scheme. As described in the introduction, the CARMENES survey has been designed to discover a statistically significant sample of exoplanets orbiting M dwarfs [Quirrenbach et al., 2014]. We have shown that CAST can optimize the survey to obtain over 67 observations per target distributed during the three years of operations. To evaluate the exoplanet yield, we have performed a number of simulations that are described below.

We simulated 100 hypothetical planet scenarios using the stellar properties available for our 309 potential targets in the CARMENES database: right ascension, declination, magnitude (which are input parameters of the scheduling algorithms) and spectral type. We used mass-luminosity relations to estimate the mass of each target. 2MASS K_s -mag and distance are taken from Carmencita [Caballero et al., 2013; Alonso-Floriano et al., 2015] to derive absolute K -band magnitudes, and masses are computed using calibrations from [Delfosse et al., 2000].

The properties of the simulated exoplanets were estimated according to the currently available exoplanet statistics. We used functional fits instead of the tables given in papers for convenience and to approximately reproduce the expected behaviour of the probability distributions with mass and period. However, these distributions should be taken with some caution given the uncertainties of planet ratio tables. The specific details for the different parameters were as follows:

- We used the mass distribution from [Mayor et al., 2011], which considers planets orbiting FGK type stars. Planet rates for M-dwarfs are also provided by [Bonfils et al., 2013], but they are based on a smaller sample of planets, thus with large uncertainties or only upper limits. However, since we are interested in M dwarfs, we scaled the planet rates of the largest mass bins in [Mayor et al.,

2011] following the statistics in [Dressing & Charbonneau, 2013]. As a smooth approximation to the binned statistics, for our simulations we fitted an exponential function to the resulting planet rates. We considered planets with masses between $1 M_{\oplus}$ and $1000 M_{\oplus}$, by extrapolating the fit below $3 M_{\oplus}$. We set a lower limit to the planet mass at $1 M_{\oplus}$ because, although we expect that sub-Earth mass planets are very abundant, their statistical distribution is not sufficiently well constrained to enter our simulations. Furthermore, such low-mass planets are unlikely to be detectable by CARMENES.

- To assign the orbital periods, we proceeded in the same way by using the planet rates for giant and large Neptune-like planets given in [Fressin et al., 2013] for simulated planets with masses above $30 M_{\oplus}$, and those given by [Dressing & Charbonneau, 2015] for smaller planets. In this case, we fitted a second order polynomial in a log-log scale to take into account the lower probability of planets on short periods. In our simulations we assumed 0.5 days as the minimum orbital period of planets.
- The eccentricity was assumed to follow the distribution presented in [Kipping, 2013].
- The inclination was taken as uniformly distributed in $\sin i$, taking into account all the possible orientations of the orbital plane.
- The argument of the periastron was assumed to follow a uniform distribution between 0 and 360 deg.
- The multiplicity of exoplanets systems was adopted to follow the Kepler Objects of Interest statistics for 1135 stars (58.9% of single planet systems, 26.5% of double planet systems, 8.6% triple, 4.3% quadruple, 1.3% quintuple, 0.2% sextuple, and 0.2% heptuple). These multiplicity rates slightly underestimate the fraction of planets per star in our simulations because of geometrical effects (narrower orbital inclination range for transits as the number of detected planets increases). However, this should not affect the conclusions of our analysis. Assuming that all stars have planets, our statistics of multiple systems predicts about 1.6 planets per star, close to the range of values given by [Gaidos et al., 2014] and [Dressing & Charbonneau, 2015]. In the case of multiple systems, for our simulations we imposed a conservative minimum ratio between planet periods of 1.3 to ensure realistic configurations in terms of orbital stability.

More details on the functional relationships and assumptions are provided in [Perger et al., 2017].

Our method to validate the scientific efficiency of the CARMENES survey using CAST is described as follows:

1. Firstly, we generated a planet scenario s as described above. For statistical significance, we simulated 100 different scenarios (N_S), i.e., 100 different planet realizations, for each of the 309 targets (N_T) in the scheduling plan described in Sect. 3. As a consistency check, we compared the statistics of our planet scenarios with those in [Bonfils et al., 2013], finding that planet ratios are in

agreement within the error bars for the planetary mass and orbital period bins relevant for our analysis.

2. For each exoplanet scenario s , we applied the 50 scheduling plans (N_R) obtained in Sect. 3. Each scheduling trial r comprises three years of observations.
3. For each target, we calculated the Keplerian radial-velocity curve that would be obtained according to the exoplanet scenario s and the observation dates of the scheduling trial r . In the case of multiple systems, we added the contribution of each planet linearly. We also included a white noise contribution to take into account the measurement uncertainty. In general, a precision of 1 m s^{-1} was considered for all targets, except for targets fainter than $J=8$ mag, for which the photon noise was assumed to scale with the magnitude from the fiducial value of 1 m s^{-1} at $J=8$ mag in 875 s.
4. In order to identify the planets that would be detected with CARMENES, we obtained the periodogram of the observations for each target following [Zechmeister & Kürster, 2009]. We labeled a planet as identified when the peak of the periodogram corresponded to the period of the planet simulated and the false alarm probability (FAP) was below the 0.1% threshold. To account for possible multiplanet systems, we subsequently computed the periodogram of the residuals subtracting the periods detected sequentially until no further significant periods were found.
5. Significant signals that did not correspond to any of the simulated planets were labeled as false positives.
6. Finally, we computed the average number of detected planets and false positive detections over all planet scenarios and scheduling trials to evaluate the efficiency on discovering planets of the simulated survey and their properties.

5.2 Results

We tested 100 different random exoplanet scenarios and obtained the average number of planet detections for 50 scheduling trials, thus adding to a total of 5000 simulations. In particular, we computed the average number of detected planets, the average number of detected planetary systems (considering that a system is detected if all its planets are found), and the average number of false positive detections. In order to assess the scientific return of the simulated survey, we analysed the number of planets that we expected to detect and their properties.

Each of the scenarios contained a different number of planets orbiting the stars selected from the Carmencita database according to the adopted planet distribution functions. On average, a total of 505^{+16}_{-17} planets were generated for each scenario. In the absence of any noise source other than photon noise, 118^{+9}_{-9} planets were detected following the usual periodogram analyses (correct period and $\text{FAP} < 0.1\%$), with $3.6^{+2.4}_{-1.6}$ planets that could be transiting. With respect to multi-planetary systems, for a total of $3.9^{+1.1}_{-1.9}$ stars all their planets were found

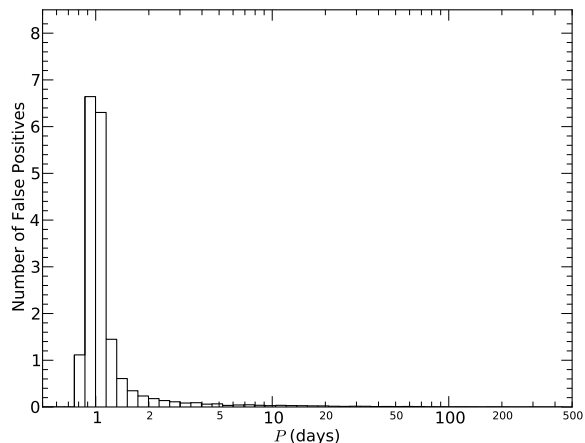


Figure 5: Histogram of the mean values of false positive detections as a function of period. The mean values are computed for the set of 5000 simulations (50 planning and 100 scenarios).

in the periodogram. Finally, there were $17.9^{+4.8}_{-4.9}$ false-positive detections, representing a false-positive rate of about 13% on average. Fig. 5 shows the distribution of false positives as a function of period. Most of these false positives correspond to the obvious 1-day sampling alias and could be readily identified and discarded. The few cases of false positives with long periods were due to residual signals from eccentric planets. All this means that the planet detection method is sensitive enough to identify planets without suffering excessively from incorrect detections.

In percentage, $23.4^{+1.9}_{-2.0}\%$ of the generated planets were detected in our simulated survey, while the average number of multiplanetary systems found was $3.1^{+1.8}_{-1.5}\%$. To understand this efficiency, one must keep in mind that a significant fraction of the simulated planets lay under the detection limit of the CARMENES instrument (in terms of radial-velocity amplitude). The top panel in Fig. 6 shows the histogram of the planet radial-velocity semi-amplitudes. The average number of generated planets and those that are detected are shown as open and shaded bars respectively. The steep decrease of the overall distribution at low amplitudes is not a physical effect, but a consequence of the limit in planet mass at $1 M_{\oplus}$. We find that exoplanet signals with semi-amplitudes exceeding 0.80 m s^{-1} can be detected with 89% probability according to our simulations.

An effect to consider in M-dwarf star surveys is the impact of magnetic activity causing so-called radial-velocity jitter [Martín et al., 2006; Prato et al., 2008]. In the CARMENES sample that we have used in our simulations, 30% of the M dwarfs show the $\text{H}\alpha$ line in emission (see Fig. 1), which is a signpost of moderate to high activity levels (Jeffers et al., submitted). To provide a rough assessment of the potential effect of activity in the CARMENES survey, we run a set of simulations by considering an additional white noise term added

in quadrature to the measurement uncertainty simulated. Although radial velocity jitter could be larger towards more active later spectral types, as a simple approach we have taken the mean noise value of 3 m s^{-1} reported in [Perger et al., 2017]. However, we recall that in our simulations the radial velocity uncertainty is also larger for these stars because they are generally fainter. The results are also shown in Fig. 6 as green bars. As expected, the radial-velocity threshold for detecting planets increases and the number of detections is reduced to about 28 planets. This is a simple approach assuming non-correlated stellar jitter. However, a thorough analysis of radial velocities using the wide wavelength interval covered by CARMENES ($0.52 \mu\text{m}$ – $1.71 \mu\text{m}$) helps to disentangle activity noise from exoplanet signals and improve the number of detections.

Fig. 6 also shows histograms for the planet mass (middle) and orbital period (bottom) of the generated and detected exoplanets (both with and without activity jitter). As expected, long-period planets are more difficult to find because the reflex radial velocities of the host stars have lower amplitudes. On the other hand, almost all planets with masses above $5 M_{\oplus}$ are above the detection threshold.

Our simulations show that the use of CAST for the planning of observations guarantees that a high percentage of the planets expected to be discovered by CARMENES could be identified. Table 6 summarizes the number and fraction of detected planets given all simulated systems and also considering the 1 m s^{-1} threshold. The results taking into account an additional 3 m s^{-1} activity jitter are also shown for comparison, but this is a worst-case scenario, as explained above.

Fig. 7 shows the probability of planet detection in the CARMENES survey as a function of stellar mass and planet semi-major axis only taking into account the measured radial velocity uncertainty. The habitable zone limits coming from the calibrations given by [Kopparapu et al., 2014] for $1 M_{\oplus}$ planets are also plotted. This figure illustrates that, as expected, the probability of detection is higher for close-in planets, but still above $\sim 25\%$ for habitable zone planets around late-type M dwarfs. As expected, if we consider also the 3 m s^{-1} stellar activity jitter, the detection probability is reduced (up to 50% in the worst cases). However, simultaneous observations using both CARMENES channels may help to correct this effect. This plot is a combination of the planet detectability using periodogram analyses and our simulated planet rates. The noisy distribution above $\sim 0.1 \text{ au}$ for low-mass stars is due to small-number statistics, since the few giant planets generated by our simulations are well above the detection threshold. Thus, if giant planets are indeed formed around late-type stars [e.g., Delfosse et al., 1998; Johnson et al., 2007] they can be easily identified, even for long period orbits.

6 Conclusions

In this paper we show that automatic scheduling algorithms are efficient tools that help to improve the outcome from exoplanet surveys by optimizing the observation planning and execution. In particular, Artificial Intelligence techniques are well suited to search for optimal solutions within the large space

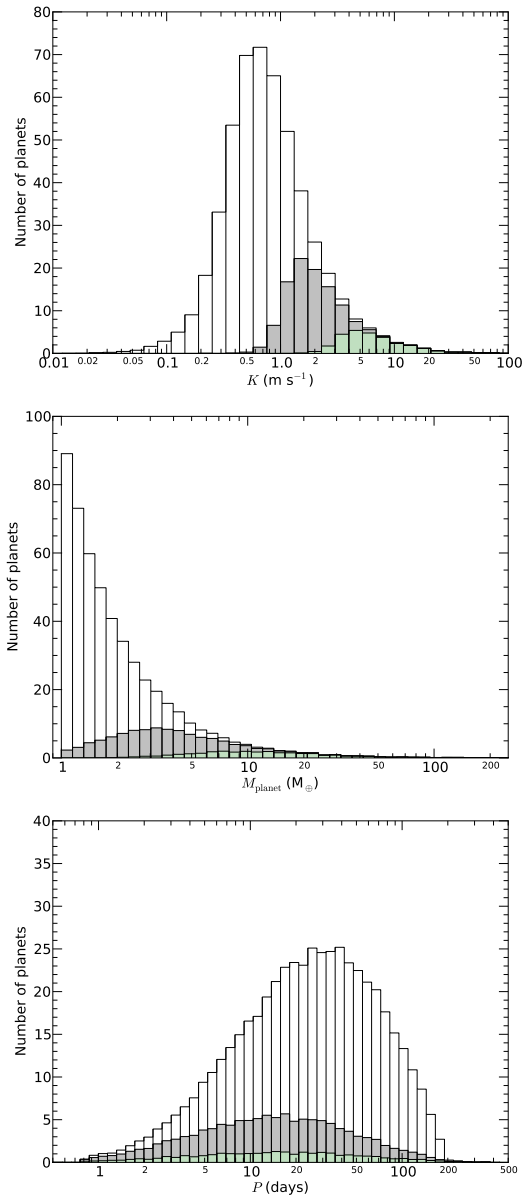


Figure 6: Histogram of the radial-velocity semi-amplitude (top), planet mass (middle) and orbital period (bottom) of the generated planets in our simulations. In all panels, open bars show the average number of simulated planets for the 100 scenarios and 50 plannings for reference. The number of detected planets assuming 1 m s^{-1} pure photon noise is shown as coloured bars. Detections with 3 m s^{-1} stellar activity jitter added to photon noise are shown in green.

Table 6: Mean values of the 50 executions of 100 planet scenarios assuming different levels of stellar intrinsic radial-velocity jitter (σ_{activity}).

σ_{activity} [m s ⁻¹]	Generated planets	Detected planets	Generated systems	Detected systems	False Positives	Detected planets (%)	Detected systems (%)
All planets							
0	505 ⁺¹⁶ ₋₁₇	118 ⁺⁹ ₋₉	126 ⁺¹¹ ₋₇	3.9 ^{+1.1} _{-1.9}	17.9 ^{+4.1} _{-4.9}	23.4 ^{+1.9} _{-2.0}	3.1 ^{+1.8} _{-1.5}
3	505 ⁺¹⁶ ₋₁₇	28 ⁺⁵ ₋₆	126 ⁺¹¹ ₋₇	0.2 ^{+2.8} _{-0.2}	4.8 ^{+2.2} _{-2.8}	5.5 ^{+1.2} _{-0.9}	0.2 ^{+2.5} _{-0.2}
Planets with $K \geq 1 \text{ m s}^{-1}$							
0	174 ⁺¹⁰ ₋₁₂	110 ⁺⁷ ₋₁₂	26 ⁺⁵ ₋₃	6.4 ^{+2.6} _{-2.4}	17.9 ^{+4.1} _{-4.9}	63.3 ^{+3.8} _{-4.0}	24.2 ^{+9.1} _{-8.1}
3	174 ⁺¹⁰ ₋₁₂	28 ⁺⁵ ₋₆	26 ⁺⁵ ₋₃	0.3 ^{+5.7} _{-0.3}	4.8 ^{+2.2} _{-2.8}	16.0 ^{+3.2} _{-2.6}	1.3 ^{+22.7} _{-1.3}

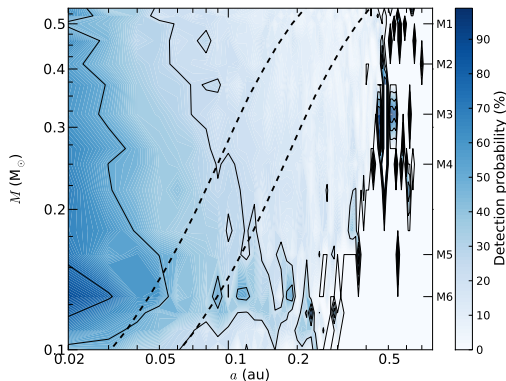


Figure 7: Probability of detection of the planets generated in CARMENES survey simulations in a semimajor axis vs. host star mass diagram. Dashed lines indicate the inner and outer habitable zone limits for $1 M_{\oplus}$ planets given in [Kopparapu et al., 2014]. Contour lines for 25, 50 and 75% detection probability are shown. For this simulation, stellar activity jitter is not taken into account. If 3 m s^{-1} jitter is added quadratically, probability is reduced by up to 50% in the worst case.

of combinations of observations, and can be adapted and generalized to any kind of survey. For the case of CARMENES we have created a scheduler, CAST, which takes into account observational constraints and distributes the telescope time amongst the different targets of the survey. We demonstrate that with the CARMENES instrument, it is possible to carry out a spectroscopic survey of a large sample of M-dwarf stars in three years. Our simulations using a list of 309 M dwarfs show that CAST optimizes the use of the instrument and can yield over 60 observations per target, fulfilling all constraints. Besides, an important advantage of using GAs in the automated scheduling process is that they guarantee a feasible, consistent, and near-optimal solution according to the constraints defined in the problem. CAST can be adapted to the needs of the astronomers in different situations during the survey and the night operation. Moreover, due to the fact that it is based on a Multi-objective Optimization Problem paradigm

by using Multi-Objective Evolutionary Algorithms, CAST is able to find optimal solutions with a trade-off between several criteria that can be in conflict with each other. This aspect provides an important advantage to CAST in order to guarantee the efficiency of the solutions in terms of use of resources (e.g., telescope operations) and in terms of science (e.g., planet detection).

In absence of noise sources other than instrumental, our simulations using recently published planet distribution statistics indicate that these observations could yield ~ 118 exoplanets above the CARMENES detection threshold. This number should be taken with caution given the still large uncertainties of planet statistics around M dwarfs, but it could be used as a reference of the planet detection efficiency. This means that about 65% of the planets causing radial-velocity semi-amplitudes larger than 1 m s^{-1} would be detectable. As expected, the number of detectable exoplanets lowers with noisier data. Assuming a radial-velocity jitter due to stellar activity of 3 m s^{-1} (white noise), the fraction of detectable planets decreases to $\sim 16\%$ for those with radial-velocity semi-amplitudes above 1 m s^{-1} , resulting in a number around 28. However, the simultaneous observation of radial velocities at optical and near-infrared wavelengths provides means to counteract this effect and permit the disentangling of planet radial-velocity signals from stellar activity. In all cases, most of the potentially detectable planets are super-Earths with masses below $10 M_{\oplus}$, and some of them in the habitable zones of their stars.

Acknowledgement

We are grateful to the referee for helpful suggestions. CARMENES is an instrument for the Centro Astronómico Hispano Alemán de Calar Alto in Almería, Spain. CARMENES is funded by the German Max-Planck-Gesellschaft (MPG), the Spanish Consejo Superior de Investigaciones Científicas (CSIC), the European Union through FEDER/ERF funds, and the members of the CARMENES Consortium (Max-Planck- Institut für Astronomie, Instituto de Astrofísica de Andalucía, Landessternwarte Königstuhl, Institut de Ciències de l’Espai, Institut für Astrophysik Göttingen, Universidad Complutense de Madrid, Thüringer Landessternwarte Tautenburg, Instituto de Astrofísica de Canarias, Hamburger Stern-

warte, Centro de Astrobiología and the Centro Astronómico Hispano-Alemán), with additional contributions by the Spanish Ministry of Economy, the state of Baden-Württemberg, the German Science Foundation (DFG), the Klaus Tschira Stiftung, and by the Junta de Andalucía. This project has received funding from the European Union's Horizon 2020 research and innovation programme under grant agreement No 653477. We also acknowledge financial support from the Spanish Ministry of Economy and Competitiveness (MINECO) through grants ESP2013-48391-C4-1-R, ESP2014-57495-C2-2-R, AYA2014-54348-C3-1-R and AYA2014-54348-C3-2-R. AR acknowledges support from the European Research Council under the FP7 Starting Grant agreement number 279347 and from DFG grant RE 1664/9-1.

References

- Akturk, M. S. & Kılıç, K. 1999, *Journal of Intelligent Manufacturing*, 10, 387
- Alonso-Floriano, F. J., Morales, J. C., Caballero, J. A., et al. 2015, *A&A*, 577, A128
- Astudillo-Defru, N., Bonfils, X., Delfosse, X., et al. 2015, *A&A*, 575, A119
- Bacardit, J. 2004, PhD thesis, *Enginyeria i Arquitectura La Salle*, Universitat Ramon Llull, Barcelona
- Bonfils, X., Lo Curto, G., Correia, A. C. M., et al. 2013, *A&A*, 556, A110
- Brown, T. M., Baliber, N., Bianco, F. B., et al. 2013, *PASP*, 125, 1031
- Burt, J., Holden, B., Hanson, R., et al. 2015, *Journal of Astronomical Telescopes, Instruments, and Systems*, 1, 044003
- Caballero, J. A., Cortés-Contreras, M., Alonso-Floriano, F. J., et al. 2013, in *Protostars and Planets VI*, Heidelberg, July 15-20, 2013. Poster #2K020
- Cesta, A., Cortellessa, G., Fratini, S., & Oddi, A. 2009, in *The 6th International Workshop on Planning and Scheduling for Space*, IWPS-09
- Civeit, T. 2013, in *Aerospace Conference*, IEEE, 1–7
- Coello Coello, C. A. 1999, *Knowledge and Information Systems*, 1, 269
- Coello Coello, C. A. 2001, in *Lecture Notes in Computer Science*, Vol. 1993, *Evolutionary Multi-Criterion Optimization*, ed. E. Zitzler, L. Thiele, K. Deb, C. A. Coello, & D. Corne (Springer), 21–40
- Coello Coello, C. A., Lamont, G. B., & Veldhuizen, D. A. V. 2007, *Evolutionary algorithms for solving multi-objective problems* (Springer-Verlag New York Inc)
- Colomé, J., Colomer, P., Guàrdia, J., et al. 2012, in *Proc. SPIE*, 8448, E1L
- Cosentino, R., Lovis, C., Pepe, F., et al. 2012, in *Proc. SPIE*, 8446, E1V
- Deb, K., Pratap, A., Agarwal, S., & Meyarivan, T. 2002, *IEEE Transactions on Evolutionary Computation*, 6, 182
- Delfosse, X., Bonfils, X., Forveille, T., et al. 2013, *A&A*, 553, A8
- Delfosse, X., Forveille, T., Mayor, M., et al. 1998, *A&A*, 338, L67
- Delfosse, X., Forveille, T., Ségransan, D., et al. 2000, *A&A*, 364, 217
- Donati, A., Reinhold, B., Martínez-Heras, J. A., & Policella, N. 2012, in *The 12th International Conference on Space Operations*
- Dressing, C. D. & Charbonneau, D. 2013, *ApJ*, 767, 95
- Dressing, C. D. & Charbonneau, D. 2015, *ApJ*, 807, 45
- Dumusque, X., Santos, N. C., Udry, S., Lovis, C., & Bonfils, X. 2011a, *A&A*, 527, A82
- Dumusque, X., Udry, S., Lovis, C., Santos, N. C., & Monteiro, M. J. P. F. G. 2011b, *A&A*, 525, A140
- Espada, D., Saito, M., Nyman, L.-A., et al. 2014, in *Proc. SPIE*, 9149, E1S
- Freedman, W. L., Hughes, S. M., Madore, B. F., et al. 1994, *AJ*, 427, 628
- Freitas, A. A. 2002, *Data Mining and Knowledge Discovery with Evolutionary Algorithms* (Secaucus, NJ, USA: Springer-Verlag New York, Inc.)
- Fressin, F., Torres, G., Charbonneau, D., et al. 2013, *AJ*, 766, 81
- Gaidos, E., Mann, A. W., Lépine, S., et al. 2014, *MNRAS*, 443, 2561
- García-Piquer, A. 2012, PhD thesis, *Enginyeria i Arquitectura La Salle*, Universitat Ramon Llull, Barcelona
- García-Piquer, A., Fornells, A., Bacardit, J., et al. 2014a, *IEEE Transactions on Evolutionary Computation*, 18, 36
- García-Piquer, A., Guàrdia, J., Colomé, et al. 2014b, in *Proc. SPIE*, 9152, E21
- García-Piquer, A., Ribas, I., & Colomé, J. 2014c, *Experimental Astronomy*, 40, 671

- Giuliano, M. E., Hawkins, R., & Rager, R. 2011, in The International Workshop on Planning and Scheduling for Space, IW PSS
- Giuliano, M. E., Rager, R., & Ferdous, N. 2007, in Proceedings of The International Conference on Automated Planning and Scheduling (AAAI), 160–167
- Goldberg, D. E. 1989, Genetic Algorithm in Search, Optimization, and Machine Learning (Addison-Wesley)
- Goldberg, D. E. 2002, The Design of Innovation: Lessons from and for Competent Genetic Algorithms (Norwell, MA, USA: Kluwer Academic Publishers)
- Holland, J. H. 1975, Adaptation in natural and artificial systems (Ann Arbor: The University of Michigan Press)
- Johnson, J. A., Butler, R. P., Marcy, G. W., et al. 2007, ApJ, 670, 833
- Kipping, D. M. 2013, MNRAS, 434, L51
- Kitching, M. & Policella, N. 2013, in The 12th Symposium on Advanced Space Technologies in Robotics and Automation
- Kopparapu, R. K., Ramírez, R. M., Schottel Kotte, J., et al. 2014, ApJl, 787, L29
- Krisciunas, K. & Schaefer, B. E. 1991, PASP, 103, 1033
- Martín, E. L., Guenther, E., Zapatero Osorio, M. R., Bouy, H., & Wainscoat, R. 2006, ApJl, 644, L75
- Mayor, M., Marmier, M., Lovis, C., et al. 2011, A&A submitted (arXiv:1109.2497)
- Mayor, M., Pepe, F., Queloz, D., et al. 2003, The Messenger, 114, 20
- Nonobe, K. & Ibaraki, T. 1998, European Journal of Operational Research, 106, 599
- Oszyczka, A. 1985, Design Optimization, 1, 193
- Pareto, V. 1897, Course d’Économie Politique, Vol. 2 (F. Pichou, Lausanne and Paris)
- Perger, M., García-Piquer, A., Ribas, I., et al. 2017, A&A, 598, A26
- Prato, L., Huerta, M., Johns-Krull, C. M., et al. 2008, ApJl, 687, L103
- Quirrenbach, A., Amado, P. J., Caballero, J. A., et al. 2014, in Proc. SPIE, 9147, EIF
- Rasconi, R., Policella, N., & Cesta, A. 2006a, in Proceedings of the ICAPS Workshop on Constraint Satisfaction Techniques for Planning and Scheduling Problems, 46–53
- Rasconi, R., Policella, N., & Cesta, A. 2006b, in Frontiers in Artificial Intelligence and Applications, Vol. 141, Proceedings of the 17th European Conference on Artificial Intelligence (IOS Press), 845–846
- Reiners, A., Bean, J. L., Huber, K. F., et al. 2010, ApJ, 710, 432
- Reiners, A., Shulyak, D., Anglada-Escudé, G., et al. 2013, A&A, 552, A103
- Sánchez, S. F., Aceituno, J., Thiele, U., Pérez-Ramírez, D., & Alves, J. 2007, PASP, 119, 1186
- Sánchez, S. F., Thiele, U., Aceituno, J., et al. 2008, PASP, 120, 1244
- Tuomi, M., Jones, H. R. A., Barnes, J. R., Anglada-Escudé, G., & Jenkins, J. S. 2014, MNRAS, 441, 1545
- Zechmeister, M. & Kürster, M. 2009, A&A, 496, 577

A Hard constraints computation

A.1 Moon influence

CAST introduces the influence of the Moon on the CARMENES survey observations by means of a merit function depending on the Moon phase and the target properties. For each potential target observation o starting at time $o_{\text{startTime}}$, the minimum accepted distance to the Moon $r(o)$ is computed as a function of the Moon phase $\phi(o_{\text{startTime}})$ (fraction of surface illuminated) following the equation

$$r(o) = ((r_{\text{min}} - 1) \cdot \phi(o_{\text{startTime}})) + 1. \quad (6)$$

where the minimum distance during full Moon is set to $r_{\text{min}}=20$ deg. For all targets farther from the Moon a hard constraint function H_{mi} is computed taking into account the Moon phase and the target magnitude following the equations

$$H_{\text{mi}}(o) = \frac{v_1(o)}{v_2(o)},$$

$$v_1(o) = 1 - \frac{m_{\text{Moon}} - m(o_{\text{target}}) \cdot (\phi(o_{\text{startTime}}))^\alpha}{m_{\text{Moon}} - m_{\text{min}} \cdot (\phi(o_{\text{startTime}}))^\alpha}, \quad (7)$$

$$v_2(o) = 1 - \frac{m_{\text{Moon}} - m_{\text{max}}}{m_{\text{Moon}} - m_{\text{min}}}.$$

where m_{moon} is the magnitude of the Moon (set to -12 mag), m_{min} and m_{max} are the minimum and maximum magnitudes of the stars in the sample and α is a power scaling factor, so that observations of faint targets close to near full-moon phases have very low priority. The denominator $v_2(o)$ is a constant scaling factor (depending on the sample) to normalize the hard constraint function H_{mi} (so that it can be as well used as a merit function if desired). All targets below a certain $H_{\text{mi}} \leq \beta$ threshold are taken into account in the scheduler. The α

and β parameters introduced in these equations are calibrated following [Krisciunas & Schaefer, 1991] and Calar Alto sky background conditions [Sánchez et al., 2008] so that targets are always five magnitudes brighter than the sky background. We find that values of $\alpha=10$ and $\beta=0.8$ satisfy this criterion.

A.2 Integration time

The estimated integration time is computed with Eq. 8, where $time_{\max}$ is the maximum integration time, t_0 is the nominal integration time, SN is the desired signal to noise ratio, SN_0 is the nominal signal to noise ratio, m_t is the magnitude of target t , and m_0 is the nominal magnitude. All values that do not depend on target t , can be parametrized as follows:

$$it(t) = \begin{cases} ct(t) & \text{if } ct(t) \leq time_{\max} \\ time_{\max} & \text{if } ct(t) > time_{\max} \end{cases}, \quad (8)$$

$$ct(t) = t_0 \cdot \left(\frac{SN}{SN_0} \right)^2 \cdot 10^{\frac{m_t - m_0}{2.5}}.$$

Reference values for this equation were computed from real CARMENES survey observations reaching $SN \sim 150$, from which radial velocities can be derived with uncertainties at the level of 1 ms^{-1} [Reiners et al., 2010]. The exposure time calibration as a function of J -band magnitude yields $SN_0=150$ for a $m_0=8$ mag star (J -band) with and exposure time $t_0=875$ s. The maximum exposure time set for any target is $time_{\max}=30$ minutes to avoid biasing the barycentric correction.

A.3 Pointing

The dome of the 3.5m telescope at the Calar Alto Observatory has a “segmented” hatch. These segments allow five open window configurations with the following apertures:

- Window 1: 9 deg–31 deg.
- Window 2: 26 deg–46 deg.
- Window 3: 42 deg–62 deg.
- Window 4: 58 deg–78 deg.
- Window 5: 73 deg–92 deg.

The scheduling algorithm takes into account this configuration of dome apertures and makes sure that the window is not obscuring the aperture during the integration. This is done by computing in advance the path of the target on the sky and the tracking of the dome during the observation. If the hatch must be moved for a particular target, such target is moved to another time slot and a different target is chosen.

A.4 Overhead time

Eq. (9) describes how to compute the prediction of the time gap (H_{not}) between the end of an observation and the beginning of a new one, where o_1 is the completed observation, o_2 is the next observation, ost is the overhead slew time for stabilization defined by the instrument properties, rot is the read-out time

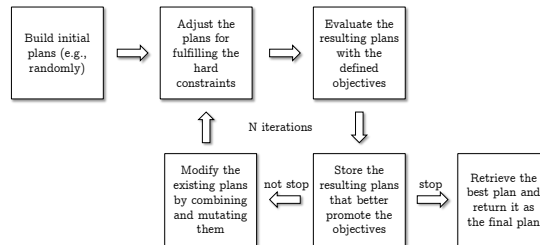


Figure 8: Cycle followed by a GA.

of the observation, and st is the slew time of the telescope that is computed by adding the time needed to move the dome (dt), the hatch (ht) and the telescope (tt) from the target of o_1 to the target of o_2 .

$$H_{\text{not}}(o_1, o_2) = \begin{cases} st(o_1, o_2), & \text{if } st(o_1, o_2) \geq rot(o_1) \\ rot(o_1), & \text{if } st(o_1, o_2) < rot(o_1) \end{cases}, \quad (9)$$

$$st(o_1, o_2) = ost + dt(o_1, o_2) + ht(o_1, o_2) + tt(o_1, o_2).$$

According to instrument and observatory specifications we assume in our calculations a telescope and dome slew rate of 1 degree per second, an stabilization overhead time $ost=120$ s, and a read out time $rot=40$ s. Finally, the dome hatch takes 60 s to change its position.

B Multi-Objective Evolutionary Algorithm design

A MOEA has four main parts: the individual representation, the genetic operators, the objective functions and the selection of the most suitable solution. As a GA, it follows the process depicted in Fig. 8.

B.1 Individual representation

In a Pittsburgh-style GA, each potential solution in the genetic process is referred to as an individual (I) and its representation is based on the definition of a genotype, which is a set of genes that can have different values, named alleles [Holland, 1975; Bacardit, 2004]. The individual genotype depends on the type of problem to solve. The first step of the algorithm randomly builds N_I individuals to be assigned to the population.

In NSGA-II [Deb et al., 2002], the individuals in the population are sorted in several fronts based on non-domination. The first front includes a set of non-dominated individuals according to the current population, the second front includes the individuals that are only dominated by the individuals in the first front, and so it continues until the last of the fronts. The individuals have a rank assigned according to the front to which they belong. Thus, individuals in the first front have a rank value of 1, individuals in the second one have a rank value of 2, and so on. For computing if an individual is dominated or non-dominated it is necessary to assign them a value for each one of the objectives evaluated in the algorithm.

B.2 Genetic operators

The GA process is roughly based on applying selection, reproduction (crossover), mutation, and replacement [Goldberg, 1989; Freitas, 2002] operators for several iterations, which are described as follows:

- *Selection.* N_S parents are selected from the current population by using a tournament selection strategy [Freitas, 2002], with a selection probability p_s , based on the rank and crowding distance. The crowding distance is a measure of how close an individual is to its neighbors according to the value of the evaluated objectives [Deb et al., 2002]. Therefore, an individual is selected if the rank is lower than the other ones or if crowding distance is greater than the other ones. After selecting the parents, the crossover and mutation operators generate two offspring for each pair of parents, obtaining N_S new individuals.
- *Crossover.* A crossover operator builds two new individuals from two previously selected parents. In our case, the two new individuals are obtained by using uniform crossover, which is based on assigning for each gene of the first child the allele of the same gene of the first parent or the second parent with a probability of 0.5. The alleles of the genes of each parent not assigned to the first child are copied in the corresponding genes of the second child. Parents are crossed with a specific p_c probability, which means that there are some situations where parents are not crossed and the two offspring are the parents themselves.
- *Mutation.* The mutation is applied to each gene of every new individual with a probability of p_μ , which means that some genes are not mutated. Usually, p_μ is a low value because only few genes have to be mutated in order to make minor changes to the individual, which is the key of diversity.
- *Replacement.* The new individuals obtained after the application of the crossover and mutation operators are evaluated according to the defined objectives. Next, they are merged with the individuals of the current population in a temporal one. The temporal population is sorted in non-dominated fronts. Next, only the best N_P individuals are added to the population used in the next generation. Individuals are selected based on their rank and on their crowding distance if they belong to the same front.

B.3 Objective functions

The definition of these figures of merit (also called fitness functions) is related to the goals of the problem (i.e., the optimization to be achieved). Moreover, in order to obtain the results in a reasonable time, these functions must imply low computational cost because they will be evaluated many times during the genetic process.

B.4 Selection of the most suitable solution

When the last generation of the NSGA-II has been achieved, the algorithm returns the optimal front of the population (i.e., all the individuals that belong to the first front, which are non-dominated by any individual of the rest of the population). This means that, considering that the algorithm has converged, there is no solution that can improve any objective without penalizing the other ones. Thus, all individuals have a different trade-off between objectives but there is no individual better than the other ones. For this reason, it is necessary to add a new step at the end of the algorithm to identify the most suitable solution according to some specific criteria.